energies

MDPI

Article

# Investigation of Corrosion Methods for Bipolar Plates for High Temperature Polymer Electrolyte Membrane Fuel Cell Application

**Nadine Pilinski [1,*], Claudia Käding [1], Anastasia Dushina [1], Thorsten Hickmann [2], Alexander Dyck [1] and Peter Wagner [1]**

[1] DLR Institute of Networked Energy Systems, Carl-von-Ossietzky-Str. 15, D-26129 Oldenburg, Germany
[2] Eisenhuth GmbH & Co. KG, Friedrich-Ebert-Straße 203, D-37520 Osterode am Harz, Germany
* Correspondence: nadine.pilinski@dlr.de; Tel.: +49-441-99906-314

Received: 14 November 2019; Accepted: 25 December 2019; Published: 3 January 2020


**Abstract:** In this work, different methods and electrochemical set-ups were investigated in order to study the corrosion behaviour of bipolar plates (BPP) for high temperature (HT) polymer electrolyte membrane fuel cell application. Using confocal and scanning electron microscopy, it was shown that chemical and electrochemical aging significantly increases surface roughness as well as morphology changes, confirming material degradation. Identical electrochemical corrosion behaviour was observed for both set-ups with typical quinone/hydroquinone peaks in the potential range ~0.6–0.7 V versus reversible hydrogen electrode (RHE). The appearance of the peaks and an increase of double layer capacitance can be related to the oxidation of carbon surface and, consequently, material corrosion. Simultaneously, an optimised corrosion set-up was introduced and verified regarding suitability. Both investigated set-ups and methods are useful to analyse the oxidation behaviour and corrosion resistance.

**Keywords:** electrochemical aging; corrosion; polymer graphite bipolar plate; polyphenylene sulphide

## 1. Introduction

The increasing interest in renewable energy sources has driven the development of high temperature polymer electrolyte membrane (HT-PEM) fuel cells (FCs) with regard to their minimal emissions, low weight, and better tolerance to fuel impurities [1,2]. Fuel cells efficiently convert chemical energy to electrical and thermal energy, while ideally using a hydrogen supply from renewable energy sources such as wind, solar, and biomass. These features allow reducing problems associated with fossil fuels, for instance, greenhouse gas emissions and air pollution, as well as a simplified system design owing to high quality heat availability [3,4].

Despite this, two main limitations concerning high cost and insufficient durability under certain operating conditions hinder the wide spread application of the HT-PEM fuel cell. Thus, a significant amount of research has been focused on the development of individual components for fuel cells including bipolar plates (BPPs), the catalyst layer, and the membrane to increase durability [3,5–11].

BPPs are one of the key components of the HT-PEM fuel cells, and play an important role in the development of fuel cell application [9,10,12]. The significance of BPPs and effect of BPP degradation on cell performance was reported by Hartnig et al. [13]. They need to fulfil many functions in a fuel cell stack, such as feeding fuel and oxidant gases through the flow field upon operation, heat transfer, and physical separation of individual fuel cells in series, and collection and transport of electrons from the anode to cathode of adjacent cells [3,5]. In order to properly perform in a fuel cell, BPPs should provide mechanical, electrical, thermal, and electrochemical stability in the environment of the system. The most common materials for manufacturing BPPs are graphite, metals, or composite-graphite.

The metallic BPPs have good mechanical stability, as well as electrical and thermal conductivity. They are smaller and lighter in comparison with the graphite materials. However, the main limitations of metal plates are their susceptibility to corrosion and dissolution in the fuel cell operating environment of 80 °C and at a pH of 2–3 [14]. Graphite BPPs offer excellent chemical stability, resistance to corrosion, low bulk resistivity, and low specific density compared with metallic BPPs. The main limitations of graphite plates are their high costs, difficulty of manufacturing, brittleness, and porosity [14].

A lot of effort has already been made to produce light-weight and cost-effective graphitic BPPs for fuel cell applications [4,15]. However, the recent BPP development has shifted from graphite to the direction of promising composite-graphite materials [16]. These type of BPPs have advantages over graphite and metallic materials regarding their low weight, flexibility, and corrosion resistance [14]. In addition, they can be produced by several economically beneficial methods including compression, transfer, or injection moulding processes [17]. The composite graphite BPPs consist of one of the conventional polymers—such as polyethylene, polypropylene, polyphenylene sulphide (PPS), or phenol formaldehyde resin—and graphite-based components, providing the mechanical stability and electrical conductivity, respectively [14]. However, some challenges, such as higher thickness and weight as well as lower electrical conductivity in comparison with metallic bipolar plates, limit the use of polymer–graphite plates in automotive application [3]. In addition, there are several reports showing that corrosion of carbon takes place under operation conditions of fuel cells [18]. The mechanism of carbon corrosion can be expressed as Equation (1) [19]:

$$C\ (s) + 2\ H_2O \rightarrow CO_2\ (g) + 4\ H^+ + 4\ e^-. \quad (1)$$

Dhakate et al. developed and tested graphite–phenolic resin composites prepared by the compression moulding technique. The corrosion resistance of material was found to be adequate as per the USA Department of Energy (US-DOE) target for the application in PEM fuel cells [20]. Kakati et al. [21] conducted a corrosion analysis in normal and rigorous simulated polymer electrolyte membrane fuel cells and alkaline fuel cell environments, and demonstrated that the corrosion current density was close to the limit set by the US-DOE. Oliveira et al. found that corrosion behaviour of PPS graphite composites depends on the carbon black concentration incorporated into the composite formulation. They revealed a trend of decreasing the corrosion resistance for higher carbon black contents associated with the porosity and electrical conductivity of the composites [4].

However, to date, only a limited number of studies about the stability of commercially available polymer–graphite BPPs and their corrosion behaviour can be found in the literature [4,15,22]. Therefore, in this study, commercial BPPs were investigated by different procedures using two electrochemical cell designs, as well as different methods. In addition, confocal microscopy and scanning electron microscopy (SEM) were used to determine surface roughness and morphological changes after the stress test.

## 2. Materials and Methods

### *2.1. BPP Samples*

The experiments were performed using compression moulded BPPs, which contain 81% carbon, 15% polyphenylene sulphide, and 4% conductive filler (PPS, Eisenhuth GmbH & Co. KG, Germany). More details cannot be disclosed because they are proprietary data of the manufacturer. The BPPs used for set-up A consisted of flow field channels and were cut into (1.4 × 1.4) $cm^2$ samples for electrochemical experiments. Owing to the cell design in set-up B, here, BPPs samples without flow field and dimensions of approximately (2.5 × 2.5) $cm^2$ and thickness of ~3 mm were used. Before experimental measurements, BPPs were cleaned in deionised water.

### 2.2. Imaging Methods

In order to investigate the surface roughness before and after the experiments, confocal microscopy measurements (Sensofar, PLu neox, Spain) were performed. The samples were scanned with 20-times magnifications and z-scan of 0.2 and 1.0 µm step size for method I and II, respectively, using the software SensoScan. The root means square surface roughness (rms) was calculated by the mentioned software after levelling the confocal microscopy image. It is defined as root mean square average of the profile height deviations from the mean line. Morphological investigations were performed by means of a scanning electron microscopy (SEM) (NEON 40, Zeiss, Germany) with 15–20 kV acceleration voltage for method I and method II and an SE2 detector.

### 2.3. Chemical and Electrochemical Aging

The following chapter will describe the electrochemical experiments of method I in a conventional (set-up A) and a newly developed set-up (set-up B) (see Figure 1). In a second experiment, set-up B will be further investigated and compared with a second chemical and electrochemical method (method II).

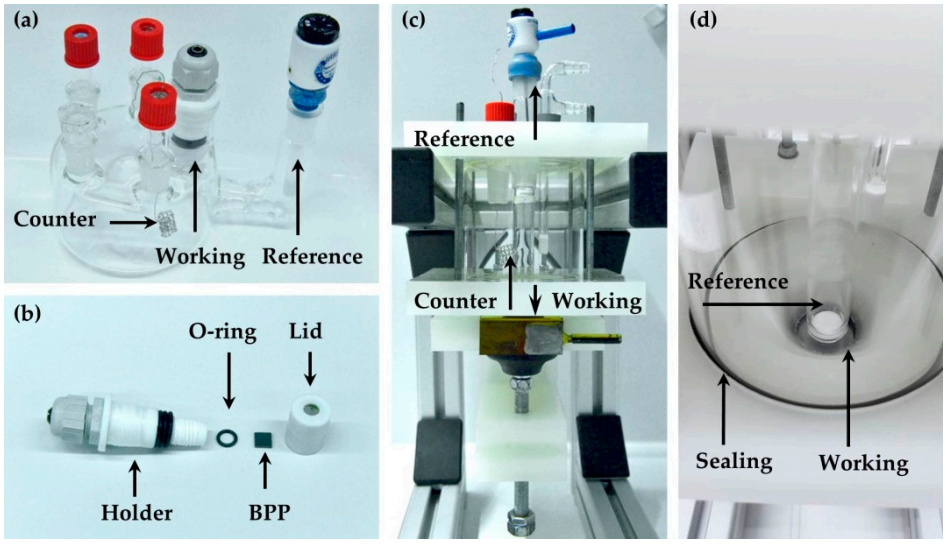


**Figure 1.** (**a**) Electrochemical set-up A; (**b**) sample holder in set-up A; (**c**) electrochemical set-up B; and (**d**) sample holder in set-up B. BPP, bipolar plate.

#### 2.3.1. Method I

Electrochemical measurements were realised in a conventional three electrode set-up inside a Faraday cage and connected to a potentiostat/galvanostat (Solartron Analytical Modulab, UK) with a BPP as the working electrode (WE), the reversible hydrogen electrode (RHE) as the reference electrode, and Pt mesh as the counter electrode. Figure 1a represents the half-cell set-up used to study the corrosion behaviour of BPPs. Such a design allows setting the working and counter electrodes as close as possible to the reference electrode. The Teflon sample holder (Figure 1b) for the BPP contains a rubber-ring for hermetic closing that allows having a proper contact for the working electrode and the Teflon lid, enabling the electrochemical response to be measured in high concentrated phosphoric acid. This set-up minimises the distance between the counter and working electrode that leads to a minimal ohmic drop between these electrodes. The active area is ~1.2 $cm^2$. The second newly developed set-up (set-up B) is shown in Figure 1c and d. The construction offers higher flexibility in corrosion tests on flat samples with larger sample sizes up to (15 × 21) $cm^2$ and an active area of up to 10 $cm^2$. In the experimental measurements shown here, an active area of ~3 $cm^2$ is used. More advantages are an optimal electrical field due to the symmetric cell design, as well as the possibility to use coated materials without destroying the coating itself.

Prior to the measurements, the electrolyte was saturated with $N_2$ for 15 min. During the measurements, $N_2$ atmosphere above the electrolyte was maintained. Pristine BPP samples were cycled for 100 cycles in the potential range from open circuit potential (OCP) to 1.2 V versus RHE in 0.5 M $H_3PO_4$ in order to pre-activate the surface. Further, BPPs were analysed by cyclic voltammetry (CV) in 0.5 M $H_2SO_4$ (>95%, Fisher Scientific, UK). Then, 0.5 M $H_2SO_4$ electrolyte was specifically selected for comparison reasons because the electrochemical behaviour of polymer–graphite composite BPPs in this media has already been reported in the literature [4,22]. A potential range from 0.25 to 1.10 V versus RHE with scan rates of 10, 20, and 50 mV $s^{-1}$ at room temperature was used for this experiment. The 10th cycle was plotted and compared for each BPP. Electrochemical aging of pristine BPPs was performed using CV in 15 M $H_3PO_4$ solution (TraceSELECT® Ultra, ≥ 85%) at room temperature in the potential range from 0.25 to 1.10 V versus RHE with a scan rate of 10 mV $s^{-1}$ for 1000 cycles. The second and last cycles were compared.

#### 2.3.2. Method II

Compared with method I, which has already been reported and whose electrochemical behaviour is well known in the literature, a second method (method II) was investigated to simulate the real HT-PEM conditions, regarding environmental as well as operational conditions. Therefore, in method II, the BPP samples were subjected to aging processes followed by potentiostatic polarisation. The chemical aging of the BPPs was achieved by immersing samples in 15 mL 15 M phosphoric acid solution at 160 °C, close to the operating temperature of HT-PEM fuel cells. The BPPs were removed from the acidic solution after 100 hours. The chemically aged BPPs were gently wiped with KIMTECH science precision wipes (Kimberly-Clark® Professional). Then, electrochemical analysis was performed using a Solartron Analytical Modulab®Xm potentiostatic/galvanostat. For the experimental set-up B, set-up A (described in Section 2.3.1.) is adapted by replacing the counter electrode consisting of a platinum wire with an activated carbon felt. RHE from Hydroflex® and larger BPP samples were used as the reference and working electrode, respectively.

The chemically-aged BPPs were analysed in the electrochemical cell at room temperature containing 15 M $H_3PO_4$ with the aim to explore the chemical stability of the BPP material composition. For electrochemical measurements, the room temperature in combination with high acid concentration was selected owing to stability limitations of the set-up. To acheive a good agreement with HT-PEM fuel cell conditions, chemical aging at higher temperatures of 160 °C was performed previously. The electrochemical measurement was run with BPP samples at three different static potentials such as open circuit potential (OCP), low polarisation potential (0.1 V vs. RHE), and high polarisation potential (0.8 V vs. RHE). Measurements were performed in $N_2$ saturated atmosphere. The low and high polarisation potentials are considered as anodic and cathodic polarisation, respectively [4]. The results of OCP over time will give an indication of the electrochemical stability of BPPs [23,24]. In order to understand the oxidation resistance of the BPPs, cyclic voltammetry was carried out within the potential range of 0 to 1.2 V at a scan rate of 20 mV $s^{-1}$ in $N_2$ atmosphere. CVs were performed with BPPs before and after aging, and after OCP, anodic and cathodic polarisation. For each static potential experiment, a new fresh electrolyte solution was used.

## 3. Results and Discussion

In the following section, the results of electrochemical characterisation of BPPs with method I in set-up A and B, as well as method II in set-up B, will be shown. Additionally, imaging methods will be displayed to correlate electrochemical properties to morphological changes.

### *3.1. Method I*

The general characterisation of pre-activated BPPs was first performed by CV in both experimental set-ups in 0.5 M $H_2SO_4$ with scan rates of 10, 20, and 50 mV $s^{-1}$. Figure 2a (set-up A) shows the typical electrochemical behaviour for carbon-based materials, while in Figure 2b (set-up B), the tilted

fish-shape behaviour can be noticed. The difference character of curves may be related to the cell geometry, while in set-up A, the WE is immersed to the electrolyte from the top and, in the case of set-up B, it is located on the bottom of the electrochemical cell. The current between the WE and RE in the case of set-up A flows horizontally, and in the case of set-up B, in the vertical direction (Figure 1). Such an important role of the RE location has already been reported in the literature by Cimenti et al. for the field of solid oxide fuel cells [25]. Further, according to the study of Battistel et al., the cell design significantly affects the impedance of electrochemical system, which may further impact the current and potential and CV curve, respectively. It was demonstrated that the use of coaxial cell geometry instead of the three electrode set-up allows to minimise the effect of electrode location on the impedance of the electrochemical system [26]. Moreover, Satola et al. found that the tilted behaviour of CV increases with aging time [22]. This could give the indication of higher degradation of BPP samples performing in set-up B. The pseudo-capacitance quinone/hydroquinone redox peaks (carbonyl and hydroxyl groups) [27–30] were clearly detected for set-up A at around 0.65 V for each scan rate, while for set-up B, the peaks are insignificant. The amount of such functionalities is an indication of the degree of surface oxidation of the BPP [22]. Furthermore, it was observed that the pseudo-capacitance increases with a higher scan rate, as expected.

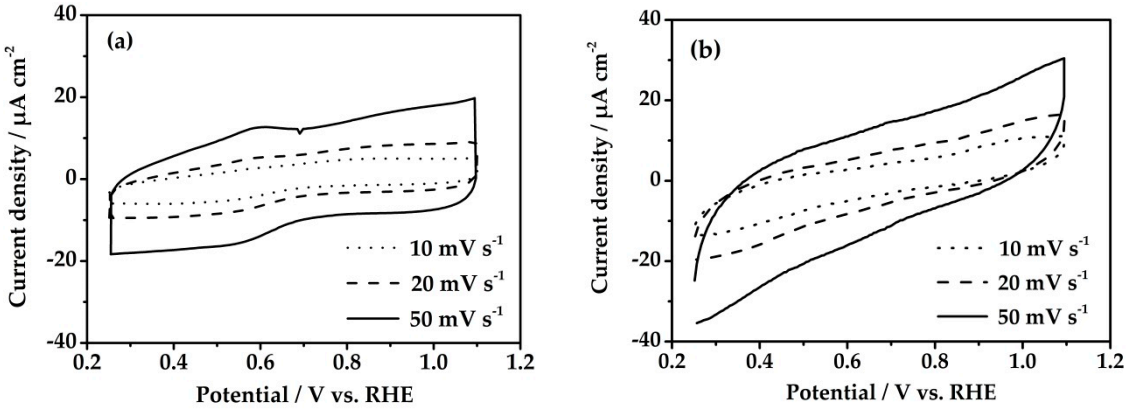


**Figure 2.** Cyclic voltammetries (CVs) of pre-activated BPPs in 0.5 M $H_2SO_4$ at different scan rates performed in experimental (**a**) set-up A and (**b**) set-up B. RHE, reversible hydrogen electrode.

The electrochemical aging was performed by applying CVs with a scan rate of 10 mV $s^{-1}$ for 1000 cycles in 15 M $H_3PO_4$. The second and 1000th CV cycles are shown in Figure 3a,b for set-up A and B, respectively. In general, the current densities before and after aging measured in set-up A are almost two times lower in comparison with those of set-up B. As already discussed above, the difference can be attributed to varied cell geometry. The size of WE for set-up B is several times higher than that for set-up A and, consequently, higher double layer capacitance may be formed between the electrode and electrolyte (Figure 1). Thus, the observed higher current density of set-up B in comparison with set-up A is a singular impact of the double layer formed on the electrode surface owing to its large electrode surface area.

It can be recognised that, for both set-ups, the pseudo-capacitance peak is located between ~0.6 and 0.7 V, which is attributed to the quinone/hydroquinone redox reaction. The peak is more pronounced after 1000 cycles in comparison with the second one, providing evidence for surface oxidation, and thus degradation of composite material. As reported in the literature, several carbon-based groups may be formed on the polymer–graphite BPP, including carbonyl, carboxyl, and esters [27–30].

To summarise the investigation of the set-up cell design with method A, it has to be mentioned that both set-ups are suitable for corrosion analysis of graphite-based materials. Typical electrochemical behaviour and pseudo-capacitance are exhibited. Nevertheless, current densities are significantly higher when performed in set-up B.

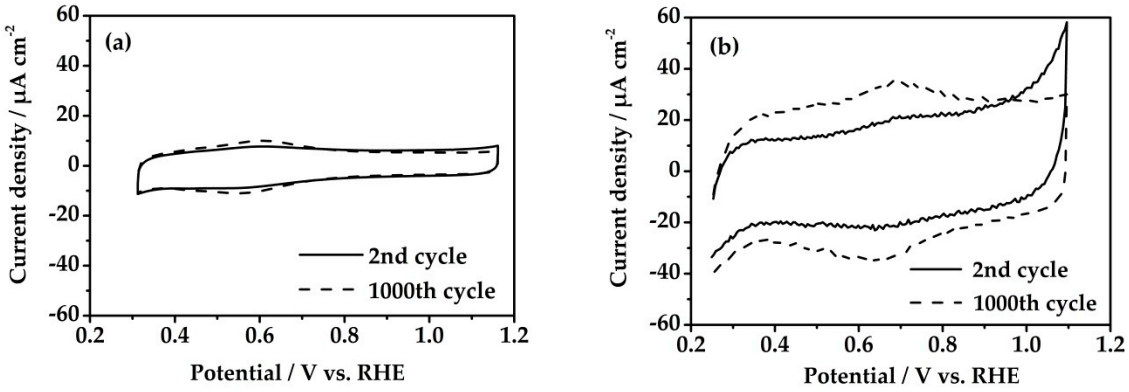


**Figure 3.** CVs of pre-activated BPPs in 15 M $H_3PO_4$ at 10 mV $s^{-1}$ performed in experimental (**a**) set-up A and (**b**) set-up B. The second and 1000th cycles are shown.

Additionally, BPP types were examined by confocal and scanning electron microscopy before and after aging in order to investigate their surface structure and morphology, respectively. Figure 4 shows confocal microscopy images and rms values of the pristine and electrochemically-aged BPPs.

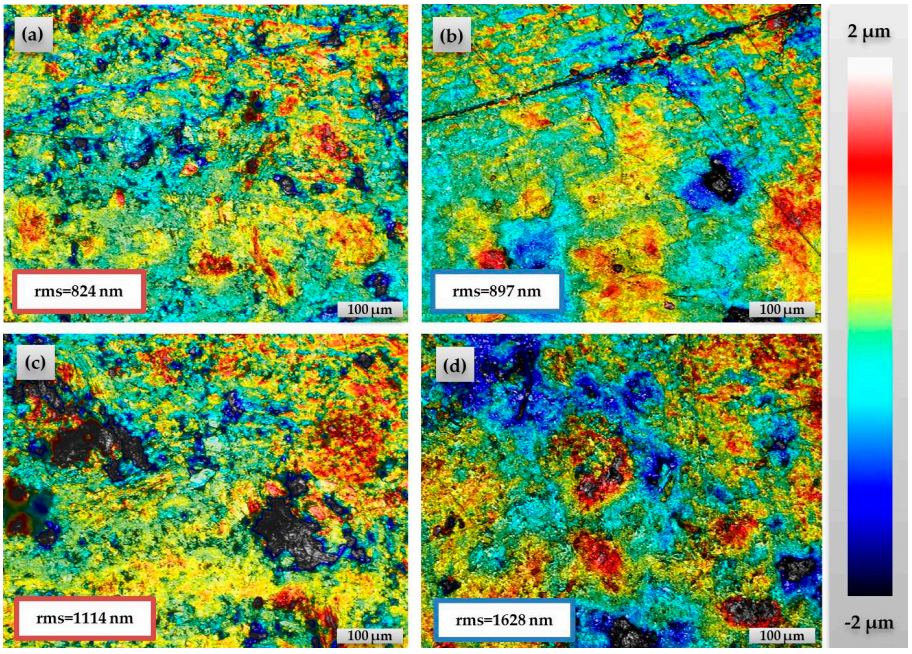


**Figure 4.** Confocal microscopy images of pre-activated BPPs in (**a**) set-up A and (**b**) set-up B, and BPPs after electrochemical aging in (**c**) set-up A and (**d**) set-up B. rms, root mean square surface roughness.

For set-up A, it can be observed that the pristine sample has a rather smooth surface with rms of 824 nm in comparison with the aged with rms of 1114 nm, which shows randomly distributed dents within the composite structure (Figure 4). Comparable roughness values with graphite composite-based bipolar plates were reported in the literature [31,32]. Analogously, detectable differences can be determined for set-up B, while the pristine samples also show a more homogeneous surface with rms of 897 nm before aging and 1628 nm after the procedure. The increase in rms is evidence for the degradation of the BPP surfaces. A similar observation was reported by Satola et al., where graphite-based BPPs were explored in terms of confocal and µ-CT measurements [22].

Figure 5 shows SEM images of the pristine BPPs and aged samples in set-up A and B. The pristine sample in set-up B contains deeper areas, but a smooth surface area overall. It is feasible that, during measurement, a deeper spot as a single defect was randomly measured, but is not representative for the total sample. It also demonstrated the variety of roughness and inhomogeneity of the graphite material.

In general, it can be observed that both pristine samples have a rather smooth surface in comparison with aged BPPs, which show randomly distributed deeper areas and deposits indicating degradation due to corrosion effects. This difference is in good agreement with the confocal microscopy analysis.

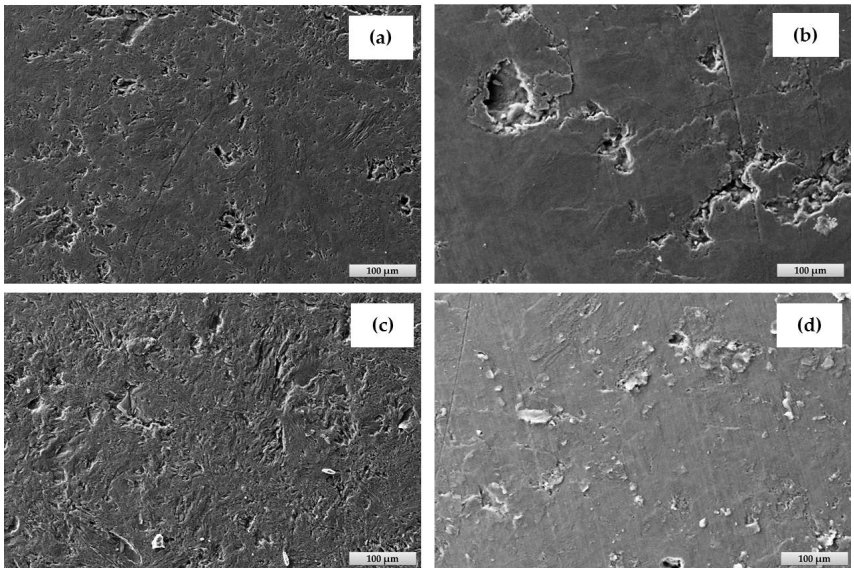


**Figure 5.** Scanning electron microscopy (SEM) images of pre-activated BPPs in (**a**) set-up A and (**b**) set-up B, and BPPs after electrochemical aging in (**c**) set-up A and (**d**) set-up B.

It can be concluded that the surface morphology and structure of BPP are closely related to the corrosion behaviour in both set-ups and can be distinguished using SEM and confocal microscopy. The dependency of roughness values and the corrosion current is also shown by Dushina et al., where similar polymer graphite BPPs were investigated in terms of electrochemical aging, and surface roughness equal to 967 nm was reported [31]. The results generated by two different corrosion cells demonstrated the importance of the set-up and the arrangement of electrodes for research on corrosion behaviour.

### *3.2. Method II*

BPPs were chemically aged in 15 M $H_3PO_4$ at 160 °C, simulating the conditions of HT-PEM fuel cells. The investigation of their electrochemical stability after aging was done by OCP over time and CV, which are mentioned as techniques to characterise the oxidation behaviour and electrochemical stability [4], and are shown in Figure 6. The steady and smooth behaviour of OCP over time (Figure 6a) gives an indication of good stability of the material [23]. Moreover, positive and stable values are associated with high stability of the electrodes and a low tendency for corrosion [24]. Oliveira et al. showed the correlation between the content of synthetic graphite and carbon black of PPS-based materials with the OCP behaviour [4]. It was confirmed that a higher carbon black concentration results in lower OCP values and increased electrochemical instability of the composites. In addition, the electrochemical stability of BPP material is verified by the CV after treatment at OCP for six hours with no significant redox peaks (Figure 6b).

In comparison with the results achieved with method I after 1000 aging cycles (Figure 3b), the graph of method II (Figure 6b) shows slightly higher current densities and allows a better verification of slight changes of BPPs regarding the corrosion behaviour.

The comparison of CVs of pristine and aged BPP samples shows an increase of double layer capacitance with respect to aging time, which can be observed in Figure 7. This result indicates a more wetted surface area owing to oxidation and higher hydrophilicity [33–35]. Moreover, higher currents can be explained by increasing roughness, resulting in more pores and penetration of electrolyte.

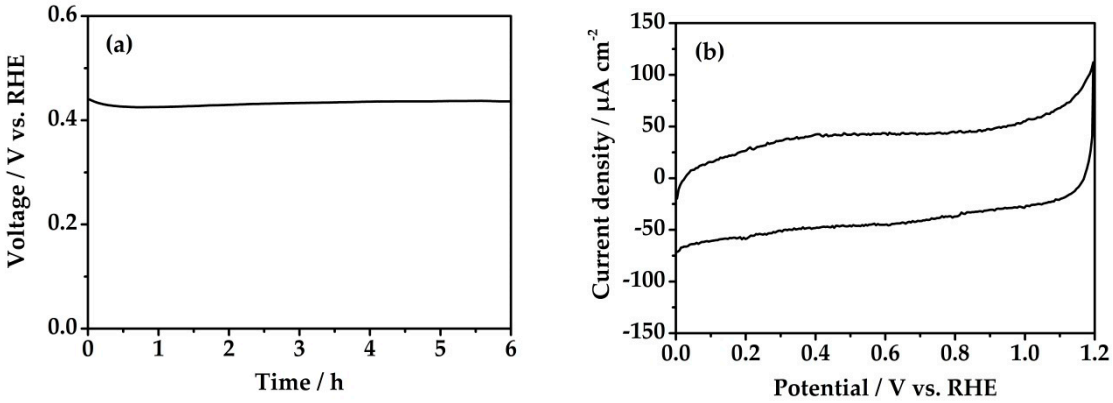


**Figure 6.** (**a**) Open circuit potential (OCP) and (**b**) CV after OCP and aging for 100 hours at 160 °C in 15 M $H_3PO_4$ with a scan rate of 20 mV $s^{-1}$. Electrochemical measurements were done in 15 M $H_3PO_4$ at room temperature.

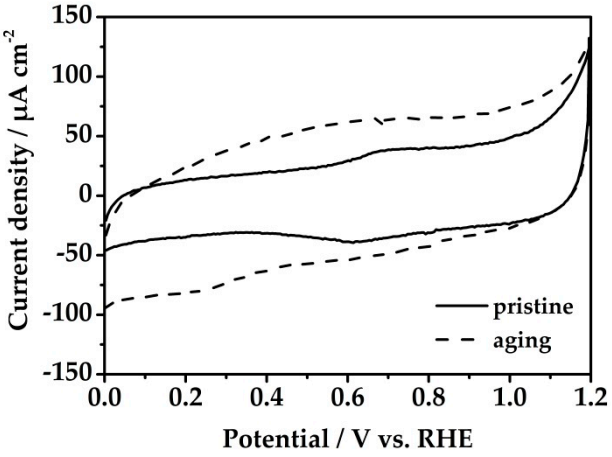


**Figure 7.** CVs before and after aging for 100 h at 160 °C in 15 M $H_3PO_4$ with a scan rate of 20 mV $s^{-1}$. Electrochemical measurements were done in 15 M $H_3PO_4$ at room temperature.

Additionally, potentiostatic measurements were performed during six hours at 0.1 and 0.8 V to simulate the PEM fuel cell anode and cathode environments, respectively (Figure 8). Published results have shown that a sulphuric acid environment was used [4]. In this work, the experiments were performed in concentrated phosphoric acid and at a temperature of 160 °C to get more realistic results regarding temperature and electrolyte in operation of the HT-PEM fuel cell system. The current density over time during both conditions is shown in Figure 8a. Positive and negative current densities were observed for cathodic and anodic polarisation, respectively, with an approach to slightly lower values. Treatment at 0.8 V indicated a current density of around 2 µA $cm^{-2}$, while polarisation at 0.1 V showed values of −2 µA $cm^{-2}$.

Further investigation of oxidation resistance performed by CVs of BPPs after treatment under anodic and cathodic conditions with method II in set-up B is shown in Figure 8b. A higher influence of cathodic conditions at 0.8 V is observed, supported by an increase of redox peak at 0.6–0.7 V, as well as double layer capacitance. This indicates a higher amount of oxygen-containing functional groups that increase the hydrophilicity of the BPP surface area [27].

For further investigation and verification of morphological changes affecting the corrosion behaviour of BPPs, imaging methods were used. The changes of surface area structure of BPP samples after different electrochemical characterisation are shown in Figures 9 and 10 by means of confocal microscopy and SEM, respectively. Additionally, rms values determined by confocal microscopy are listed.

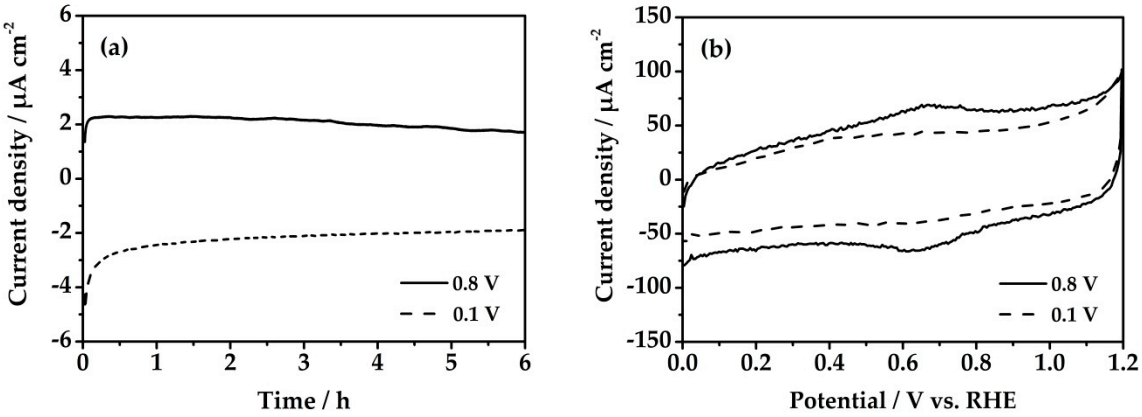


**Figure 8.** (**a**) Current density over time and (**b**) CVs after anodic (0.1 V) and cathodic (0.8 V) conditions after aging for 100 hours at 160 °C in 15 M $H_3PO_4$. Electrochemical measurements were done in 15 M $H_3PO_4$ at room temperature.

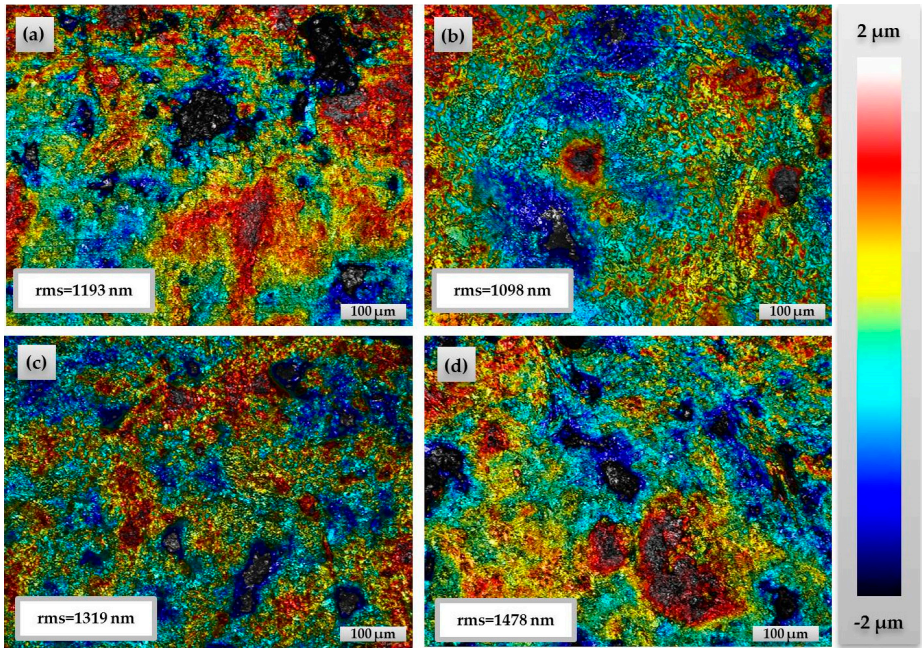


**Figure 9.** Confocal microscopy images of BPP (**a**) after aging, and after potentiostatic measurements at (**b**) OCP, (**c**) 0.1 V, and (**d**) 0.8 V.

The results verify the above-mentioned corrosion behaviour after aging and potentiostatic treatment, as higher roughness at the surface area can be detected. Similar corrosion and increased roughness after aging is observed with method I, but with a higher effect on morphological changes compared with method II. However, comparing the results performed with method II, a less flat and smooth surface, as well as a growth of deeper areas in comparison with pristine samples with 897 nm, is visible. This is confirmed by an increase of rms values and can provide the indication that, through the roughening of the surface, more pores were formed, resulting in higher uptake of electrolyte and less corrosion resistance. SEM images supported the results and displayed a less smooth surface area with an increase of cracks. The surface area detected by SEM after potentiostatic measurements of OCP, 0.1, and 0.8 V is more or less comparable with slightly higher changes after anodic conditions at 0.1 V (Figure 10). Nevertheless, the confocal microscopy analysis indicates an increase of larger and deeper holes at the surface area after cathodic conditions. The rms value increased with 1478 nm in comparison with pristine with 897 nm. This is in a good agreement with the results of the electrochemical characterisation. Oxidation of the surface area, which was observed through

the quinone/hydroquinone redox activity in the CV, induced hydrophilicity [22]. Oliveira et al. [4] reported that SEM images did not reveal any significant changes of morphological characteristics, but an increase of internal voids led to corrosion. Satola et al. [28] concluded with the assumption that SEM and confocal microscopy only give evidence about the surface roughness changes, but not about morphological changes of the bulk material. It is also shown that the corrosion behaviour is strongly affected by an increase of porosity.

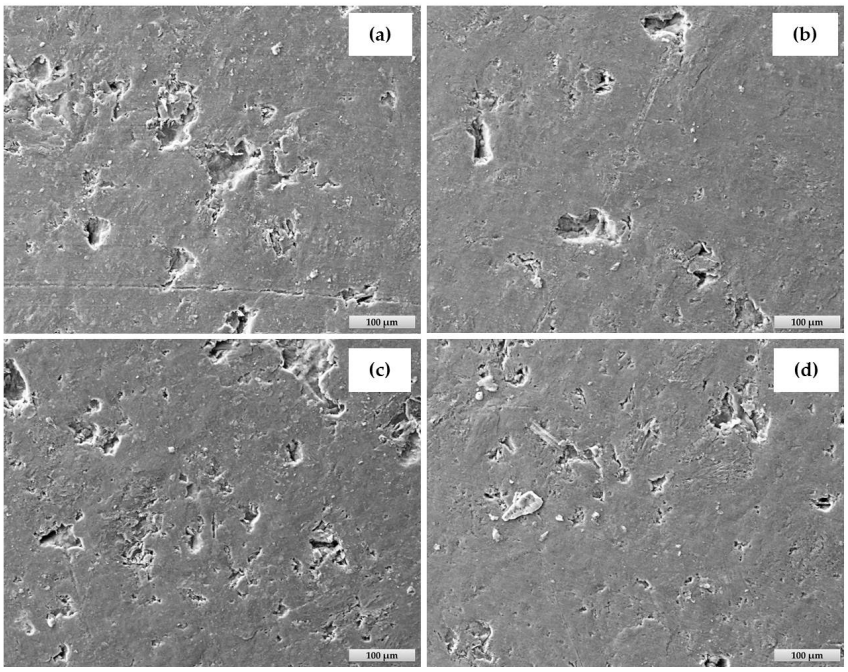


**Figure 10.** SEM images of BPP (**a**) after aging, and after potentiostatic measurements at (**b**) OCP, (**c**) 0.1 V, and (**d**) 0.8 V.

## 4. Conclusions

In this work, BPP corrosion behaviour was investigated and optimised in terms of chemical and electrochemical aging for HT-PEM fuel cell application. Therefore, the results of well-known and newly developed methods and electrochemical set-ups were investigated. Additionally, imaging methods were shown to correlate electrochemical properties to morphological changes.

A conventional three-electrode set-up was utilised for experiments referred to as set-up A, and an optimised cell was referred to as set-up B, where an arrangement for flexible use of BPP was employed. The electrochemical measurements in set-up A and B were done by operating 1000 aging cycles in 15 M $H_3PO_4$ (method I). Typical electrochemical behaviour and pseudo-capacitance are exhibited in both set-ups and can be associated with the oxidation of graphite and, therefore, material degradation. This can be confirmed by scanning electron and confocal microscopy analyses. The surface morphology and structure of the BPP are closely related to the corrosion behaviour in both set-ups.

Method II was optimised for a high temperature PEM fuel cell environment and operation condition, where BPPs were chemically aged in 15 M $H_3PO_4$ at 160 °C and potentiostatic treated at OCP, 0.1, and 0.8 V. The oxidation behaviour and electrochemical stability showed a decrease after aging and treatment at cathodic conditions at 0.8 V, confirmed by the increase of double layer capacitance and/or redox peak formation associated with material corrosion. This observation can be confirmed by surface morphology changes. Moreover, method II revealed higher current density after aging compared with method I, while the redox peaks at ~0.6–0.7 V were not clearly pronounced. Further investigations have to be done to evaluate the effect of lifetime of a fuel cell stack.

Overall, it was demonstrated that the newly developed method and set-up can be used for the investigation of the electrochemical corrosion of polymer graphite BPP, while the results are in a good

agreement with each other, suggesting promising applications of these techniques for studying the corrosion behaviour of commercially available BPPs in HT-PEM fuel cells.

**Author Contributions:** Conceptualization, N.P., C.K. and A.D. (Anastasia Dushina); investigation, N.P., C.K. and A.D. (Anastasia Dushina); writing—original draft preparation, N.P., C.K. and A.D. (Anastasia Dushina); writing—review and editing, T.H., A.D. (Alexander Dyck) and P.W.; supervision, A.D. (Alexander Dyck). All authors have read and agreed to the published version of the manuscript.

**Funding:** This research was funded by the German Federal Ministry of Transport and Digital Infrastructure (BMVI) within the project BEPPEL, grant number 03B110002A2, and the German Federal Ministry for Economic Affairs and Energy (BMWi) within the project QUALIFIX, grant number 03Et6046A.

**Acknowledgments:** The authors would like to thank Stefanie Laue and Khrystyna Yezerska for their support.

**Conflicts of Interest:** The authors declare no conflict of interest.

## References

1. Rosli, R.E.; Sulong, A.B.; Daud, W.R.W.; Zulkifley, M.A.; Husaini, T.; Rosli, M.I.; Majlan, E.H.; Haque, M.A. A review of high-temperature proton exchange membrane fuel cell (HT-PEMFC) system. *Int. J. Hydrogen Energy* **2017**, *42*, 9293–9314. [CrossRef]
2. Chandan, A.; Hattenberger, M.; El-Kharouf, A.; Du, S.; Dhir, A.; Self, V.; Pollet, B.G.; Ingram, A.; Bujalski, W. High temperature (HT) polymer electrolyte membrane fuel cells (PEMFC)—A review. *J. Power Sources* **2013**, *231*, 264–278. [CrossRef]
3. Araya, S.S.; Zhou, F.; Liso, V.; Sahlin, S.L.; Vang, J.R.; Thomas, S.; Gao, X.; Jeppesen, C.; Kær, S.K. A comprehensive review of PBI-based high temperature PEM fuel cells. *Int. J. Hydrogen Energy* **2016**, *41*, 21310–21344. [CrossRef]
4. Lopes de Oliveira, M.C.; Sayeg, I.J.; Ett, G.; Antunes, R.A. Corrosion behavior of polyphenylene sulfide–carbon black–graphite composites for bipolar plates of polymer electrolyte membrane fuel cells. *Int. J. Hydrogen Energy* **2014**, *39*, 16405–16418. [CrossRef]
5. Cruz-Gonzales, T. *Theory of Proton Exchange Membranes Fuel Cells and the Testing of Performance Characteristics of Polymer Electrolyte Membranes*; Massachuesetts Institute of Technology: Cambridge, MA, USA, 2004.
6. Asensio, J.A.; Sanchez, E.M.; Gomez-Romero, P. Proton-conducting membranes based on benzimidazole polymers for high-temperature PEM fuel cells. A chemical quest. *Chem. Soc. Rev.* **2010**, *39*, 3210–3239. [CrossRef]
7. De Bruijn, F.A.; Dam, V.A.T.; Janssen, G.J.M. Review: Durability and degradation issues of PEM fuel cell components. *Fuel Cells* **2008**, *8*, 3–22. [CrossRef]
8. Kuan, H.-C.; Ma, C.-C.M.; Chen, K.H.; Chen, S.-M. Preparation, electrical, mechanical and thermal properties of composite bipolar plate for fuel cell. *J. Power Sources* **2004**, *134*, 7–17. [CrossRef]
9. Hermann, A.; Chaudhuri, T.; Spagnol, P. Bipolar plates for PEM fuel cells: A review. *Int. J. Hydrogen Energy* **2005**, *30*, 1297–1302. [CrossRef]
10. Cunningham, B.D.; Huang, J.; Baird, D.G. Development of bipolar plates for fuel cells from graphite filled wet-lay material and a thermoplastic laminate skin layer. *J. Power Sources* **2007**, *165*, 764–773. [CrossRef]
11. Alegre, C.; Álvarez-Manuel, L.; Mustata, R.; Valiño, L.; Lozano, A.; Barreras, F. Assessment of the durability of low-cost Al bipolar plates for High Temperature PEM fuel cells. *Int. J. Hydrogen Energy* **2019**, *44*, 12748–12759. [CrossRef]
12. Barreras, F.; Lozano, A.; Roda, V.; Barroso, J.; Martín, J. Optimal design and operational tests of a high-temperature PEM fuel cell for a combined heat and power unit. *Int. J. Hydrogen Energy* **2014**, *39*, 5388–5398. [CrossRef]
13. Hartnig, C.; Schmidt, T.J. On a new degradation mode for high-temperature polymer electrolyte fuel cells: How bipolar plate degradation affects cell performance. *Electrochim. Acta* **2011**, *56*, 4237–4242. [CrossRef]
14. Rungsima, Y.; Michael, F.; Costas, T. A review of thermoplastic composites for bipolar plate materials in pem fuel cells. In *Nanocomposites with Unique Properties and Applications in Medicine and Industry*; Cuppoletti, J., Ed.; Intech: Vienna, Austria, 2011; pp. 317–344. [CrossRef]
15. Hamilton, P.J.; Pollet, B.G. Polymer electrolyte membrane fuel cell (PEMFC) flow field plate: Design, materials and characterisation. *Fuel Cells* **2010**, *4*, 489–509. [CrossRef]

16. Taherian, R. A review of composite and metallic bipolar plates in proton exchange membrane fuel cell: Materials, fabrication, and material selection. *J. Power Sources* **2014**, *265*, 370–390. [CrossRef]
17. Antunes, R.A.; de Oliveira, M.C.L.; Ett, G.; Ett, V. Carbon materials in composite bipolar plates for polymer electrolyte membrane fuel cells: A review of the main challenges to improve electrical performance. *J. Power Sources* **2011**, *196*, 2945–2961. [CrossRef]
18. Engl, T.; Gubler, L.; Schmidt, T.J. Think different! Carbon corrosion mitigation strategy in high temperature PEFC: A rapid aging study. *J. Electrochem. Soc.* **2015**, *162*, F291–F297. [CrossRef]
19. Rodrigues Castanheira, L.F. Corrosion of High Surface Area Carbon Supports Used in Proton-Exchange Membrane Fuel Cell Electrodes. Ph.D. Thesis, Université de Grenoble, Grenoble, France, 2014.
20. Dhakate, S.R.; Mathur, R.B.; Kakati, B.K.; Dhami, T.L. Properties of graphite-composite bipolar plate prepared by compression molding technique for PEM fuel cell. *Int. J. Hydrogen Energy* **2007**, *32*, 4537–4543. [CrossRef]
21. Kakati, B.K.; Sathiyamoorthy, D.; Verma, A. Electrochemical and mechanical behavior of carbon composite bipolar plate for fuel cell. *Int. J. Hydrogen Energy* **2010**, *35*, 4185–4194. [CrossRef]
22. Satola, B.; Komsiyska, L.; Wittstock, G. Corrosion of graphite-polypropylene current collectors during overcharging in negative and positive vanadium redox flow battery half-cell electrolytes. *J. Electrochem. Soc.* **2018**, *165*, A963–A969. [CrossRef]
23. Wang, L.-N.; Luo, J.-L. Electrochemical behaviour of anodic zirconium oxide nanotubes in simulated body fluid. *Appl. Surf. Sci.* **2012**, *258*, 4830–4833. [CrossRef]
24. Bolat, G.; Mareci, D.; Chelariu, R.; Izquierdo, J.; González, S.; Souto, R.M. Investigation of the electrochemical behaviour of TiMo alloys in simulated physiological solutions. *Electrochim. Acta* **2013**, *113*, 470–480. [CrossRef]
25. Cimenti, M.; Co, A.C.; Birss, V.I.; Hill, J.M. Distortions in Electrochemical Impedance Spectroscopy Measurements Using 3-Electrode Methods in SOFC. I—Effect of Cell Geometry. *Fuel Cells* **2007**, *7*, 364–376. [CrossRef]
26. Battistel, A.; Fan, M.; Stojadinović, J.; La Mantia, F. Analysis and mitigation of the artefacts in electrochemical impedance spectroscopy due to three-electrode geometry. *Electrochim. Acta* **2014**, *135*, 133–138. [CrossRef]
27. Satola, B.; Kirchner, C.N.; Komsiyska, L.; Wittstock, G. Chemical stability of graphite-polypropylene bipolar plates for the vanadium redox flow battery at resting state. *J. Electrochem. Soc.* **2016**, *163*, A2318–A2325. [CrossRef]
28. Satola, B.; Komsiyska, L.; Wittstock, G. Bulk aging of graphite-polypropylene current collectors induced by electrochemical cycling in the positive electrolyte of vanadium redox flow batteries. *J. Electrochem. Soc.* **2017**, *164*, A2566–A2572. [CrossRef]
29. Kinoshita, K.; Bett, J.A.S. Potentiodynamic analysis of surface oxides on carbon blacks. *Carbon* **1973**, *11*, 403–411. [CrossRef]
30. Choo, H.-S.; Kinumoto, T.; Jeong, S.-K.; Iriyama, Y.; Abe, T.; Ogumi, Z. Mechanism for electrochemical oxidation of highly oriented pyrolytic graphite in sulfuric acid solution. *J. Electrochem. Soc.* **2007**, *154*, B1017–B1023. [CrossRef]
31. Dushina, A.; Satola, B.; Dyck, A.; Wagner, P. Comparative investigation of polyphenylene sulfide polymer-graphite bipolar plates for fuel cell application. *ECS Trans.* **2019**, *92*, 361–373. [CrossRef]
32. Lee, H.S.; Kim, H.J.; Kim, S.G.; Ahn, S.H. Evaluation of graphite composite bipolar plate for PEM (proton exchange membrane) fuel cell: Electrical, mechanical, and molding properties. *J. Mater. Process. Technol.* **2007**, *187–188*, 425–428. [CrossRef]
33. Jaiswal, A.; Chalasani, S.C. The role of carbon in the negative plate of the lead–acid battery. *J. Energy Storage* **2015**, *1*, 15–21. [CrossRef]
34. Goulet, M.-A.; Skyllas-Kazacos, M.; Kjeang, E. The importance of wetting in carbon paper electrodes for vanadium redox reactions. *Carbon* **2016**, *101*, 390–398. [CrossRef]
35. Chmiola, J.; Yushin, G.; Dash, R.K.; Hoffman, E.N.; Fischer, J.E.; Barsoum, M.W.; Gogotsi, Y. Double-layer capacitance of carbide derived carbons in sulfuric acid. *Electrochem. Solid State Lett.* **2005**, *8*, A357–A360. [CrossRef]